ELSEVIER

Tectonophysics 312 (1999) 97–115

TECTONOPHYSICS

www.elsevier.com/locate/tecto

An integrated model for transitional pressure solution in sandstones

F. Renard [a,c,*], A. Park [b], P. Ortoleva [b], J.-P. Gratier [a]

[a] *LGIT, CNRS–Observatoire, Université Joseph Fourier, IRIGM BP 53, 38041, Grenoble, France*
[b] *Departments of Chemistry and of Geological Sciences, Indiana University, Bloomington, IN 474057 USA*
[c] *Institute of Geology and Department of Physics, Postboks 1047 Blindern, N-0316 Oslo, Norway*

Received 9 March 1998; accepted 9 June 1999

Abstract

A key aspect of the deformation of sedimentary rocks during diagenesis is pressure solution. However, it is often not clear why some rocks of a given mineralogy, depth, and pressure exhibit a great deal of pressure solution while very similar rocks under similar conditions do not. To address such difficulties, which we believe arise from the natural, non-linear physico-chemical processes, a quantitative model for pressure solution applied to sandstones has been developed. This model subsumes various factors: (1) pressure, temperature, and burial rate; (2) grain size, shape, and packing of the mineral grains; (3) the variability of water film thickness and coefficient of diffusion between any two grains in contact as a function of stress across the contact, pore fluid pressure, salinity, pH, and temperature. In this study we distinguish several types of surface sites over quartz grains in a sandstone with corresponding differences in chemical potential, thus allowing the diffusive transfer of matter from one site to another. The contact between two grains is divided into two parts. The actual true contact between two grains is a site of 'water film diffusion', and the inclusions inside the contact, the free-face inclusion contacts, are sites of 'free-face pressure solution'. On the pore surface site, precipitation occurs. It is shown that a kinetics transition from a reaction-limited deformation to a diffusion-limited deformation occurs in the upper crust. A geometric transition occurs too due to the textural evolution of the rock with deformation. The main goal of this paper is to show the dynamics of the shifting importance of actual and free-face inclusion contacts using a unified model including both features. The result is a predictive model for porosity variations with depth due to pressure solution in sandstones.

Keywords: sandstone; compaction; porosity; pressure solution; grain contact; fluid inclusions

1. Introduction

The deformation of sedimentary rocks by pressure solution has been recognized for many years (Heald, 1955; Weyl, 1959; Engelder, 1982). This mechanism is responsible of a viscous creep of rocks in the upper crust (Urai et al., 1986). Several mechanistic models have been proposed, three models of which are reviewed in the following:

In the first 'water film diffusion' (WFD) model mineral dissolution is assumed to take place at the grain–grain contact area with the solutes diffusing along an adsorbed water film layer. The precipitation of the solute occurs on the pore surface (Weyl, 1959; Rutter, 1976). The driving force for this deformation is a difference of normal stress between the grain

* Corresponding author. E-mail: francois@geologi.uio.no

0040-1951/99/$ – see front matter
PII: S0040-1951(99)00202-4

contact and the pore. In this case, dissolution at the contact is stress-enhanced.

In the second, 'free-face pressure solution' (FFPS) model, dissolution occurs at the margins of the contacts, leading to undercutting and the eventual brittle or plastic deformation taking place within the contact (Bathurst, 1958; Tada et al., 1987). In this model, dissolution is strain-enhanced.

In the third model, it is proposed that the nominal contact between two grains is not flat and can contain channel and island structures at a nanometer scale (Raj and Chyung, 1981) or at a micron scale (Spiers et al., 1990; Gratz and Bird, 1993a,b). Between the channels, plastic or brittle deformations can take place.

In this paper, we try to reconcile these three models by using a formulation of the pressure solution mechanism that subsumes both 'water film diffusion' and 'free-face pressure solution' mechanisms in a framework of channels or corrugated grain contacts. This new model integrates all the steps of the deformation: dissolution at grain interface, diffusion of matter along the interface and precipitation in the pore space. The modification of pore space due to neck growth (sintering) as observed in an experiment by Hickman and Evans (1991) will not be incorporated in our model.

A crucial parameter for pressure solution is the presence of water in the pores because it is the medium of transport and reaction with the minerals (Rutter, 1976). If a porous medium is not saturated with respect to water, pressure solution will be localized in the pores where water is present. This effect can create compacted regions in the sediment whereas the porosity of other regions will not be modified.

2. Rock texture model

The non-linear dynamics of pressure solution and compaction process arise from the fact that during deformation intergranular contact areas grow. To take in account such geometric evolution, the rock is modeled as a cubic array of grains (Dewers and Ortoleva, 1990; Ortoleva, 1994) and assumed to be a monomineralic sandstone. The grains of quartz have a truncated spherical geometry (Figs. 1 and 2) which

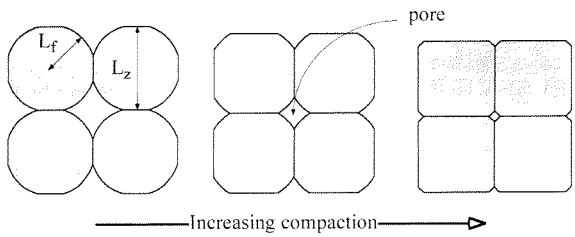

Fig. 1. A cross-section view of a cubic-packed network of truncated spheres. The grain shapes evolve due to pressure solution as shown: the grain radius L_f increases while the grain flattens (L_z decreases) resulting in the porosity and the pore surface decrease.

is characterized by four geometrical lengths: L_f, the grain radius, and L_x, L_y, and L_z, the lengths of the truncations in the three directions of space (Fig. 2). The grains have nominal grain–grain contacts with internal structures (Spiers et al., 1990; Spiers and Schutjens, 1990; Schutjens, 1991) which consist of a number of free-face inclusion contacts (similar to fluid inclusions) that evolve via FFPS. The regions between these fluid inclusions, the actual true contacts, evolve via a WFD mechanism (Figs. 3 and 4). When the number of inclusions is small, they are assumed to be isolated, whereas when their number increases they can connect together, forming small channels. Stress-enhanced dissolution, mostly due to the normal stress effect, occurs in the actual true con-

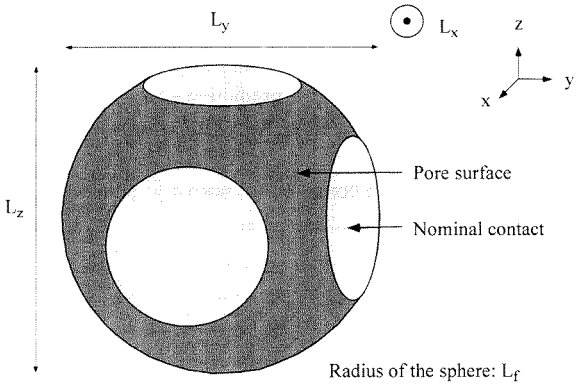

Fig. 2. Detailed description of the truncated spheres of Fig. 1. The dark gray region is the pore surface whereas the lighter gray regions correspond to areas in contact with other grains. Each contact represents the composite nominal contact of Fig. 3. The variables are used in Eqs. 1 and 3. Grain radius, L_f ($L_f > 2L_x$, $2L_y$, $2L_z$), can vary from micrometers (siltstones) to millimeters (sandstones).

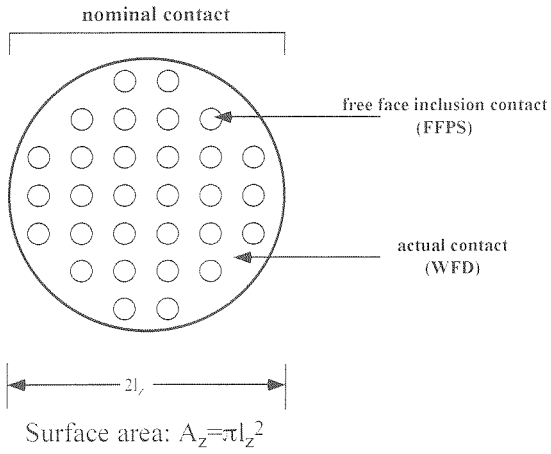

Fig. 3. A view of a structured nominal contact between two grains. The surface area of the contact is A_z as shown. Actual contacts deform according to the 'water film diffusion' (WFD) mechanism, whereas free-face contacts (inclusions) deform according to the 'free-face pressure solution' (FFPS) mechanism. The free-face contacts can overlap, allowing connection all over the nominal contact.

tacts. Strain-enhanced dissolution (plastic and elastic dissolution) occurs in the free-face inclusion contacts and in the pore space. Some of these inclusions can be located at the outer perimeter of the contact allowing FFPS there.

The pressure in the pore space is assumed to be hydrostatic, i.e. there is no overpressure in the pore. On the opposite, inside the fluid inclusions, fluid pressure is allowed to build-up if the inclusions become closed and no more connected to the pore. With these assumptions and the corresponding driving forces, a transition between the WFD and FFPS behaviors is shown to occur due to the modifications of solute mobility along the water film at the contacts with stress and temperature variations.

3. Transitional pressure solution approach

Our model takes into account different sites on the surface of a grain and the exchange of matter between them (Gratz, 1991; Wakai, 1994; Lehner, 1995; Renard et al., 1997). The overall mechanism can be described in three steps (Fig. 5). First, dissolution occurs in the actual true contacts. Secondly aqueous silica is transported by diffusion along the adsorbed water film. This second step comprises two parts in parallel. It takes into consideration diffusion from the actual contacts to the pore fluid and diffusion from the actual contacts to the free-face inclusion contacts where precipitation or dissolution can occur, decreasing or increasing the volume and surface area of the inclusions (Figs. 3, 5 and 6). This diffusion step is made significantly more effective if the free-face inclusion contacts are connected and form channels. As the third and last step, silica precipitation can take place on the pore surface.

3.1. Geometrical model and compaction

For simplicity of the presentation, we will focus on the vertically directed grain contacts (normal to the z-axis) (Fig. 2). Results are identical for the horizontally directed contacts (normal to x and y contacts) because one considers an isotropic loading of the system. This assumption of an isotropic load is fair in the geological conditions of a sedimentary basin. As shown in Figs. 3 and 4 the nominal contact of a grain contains an actual true contact surface and a free-face inclusion contact surface. The latter is modeled as an array of conical inclusions (Fig. 4) of height ξ_z and radius of the base ψ_z. The cones are assumed to have a constant angle of 90°, therefore ξ_z and ψ_z are equal (Fig. 4a). This array of conical inclusions inside a planar actual contact is assumed to describe the complex contact of the island and channel model of Spiers et al. (1990). If inclusions are large enough, they can become connected, allowing for direct matter transport from the grain contacts to the pore.

To complete the textural descriptions the following quantities (Figs. 2–4) are introduced:

A_z	nominal contact area (m^2) (Fig. 3).
l_z	nominal contact area radius (m) (Fig. 3).
L_x, L_y, L_z	truncations for the spherical grains in the three directions of space (m) (Fig. 2).
L_f	radius of the spherical grain (m) (Fig. 2).
a_z	area fraction of one of the actual contacts within the nominal contact (Fig. 4b).
n_z	number of inclusions (free-face inclusion contacts) per nominal contact area.
A_p	pore surface area (m^2).
P_n	normal stress to a solid surface.
p_p	fluid pressure in the open pore (bar).

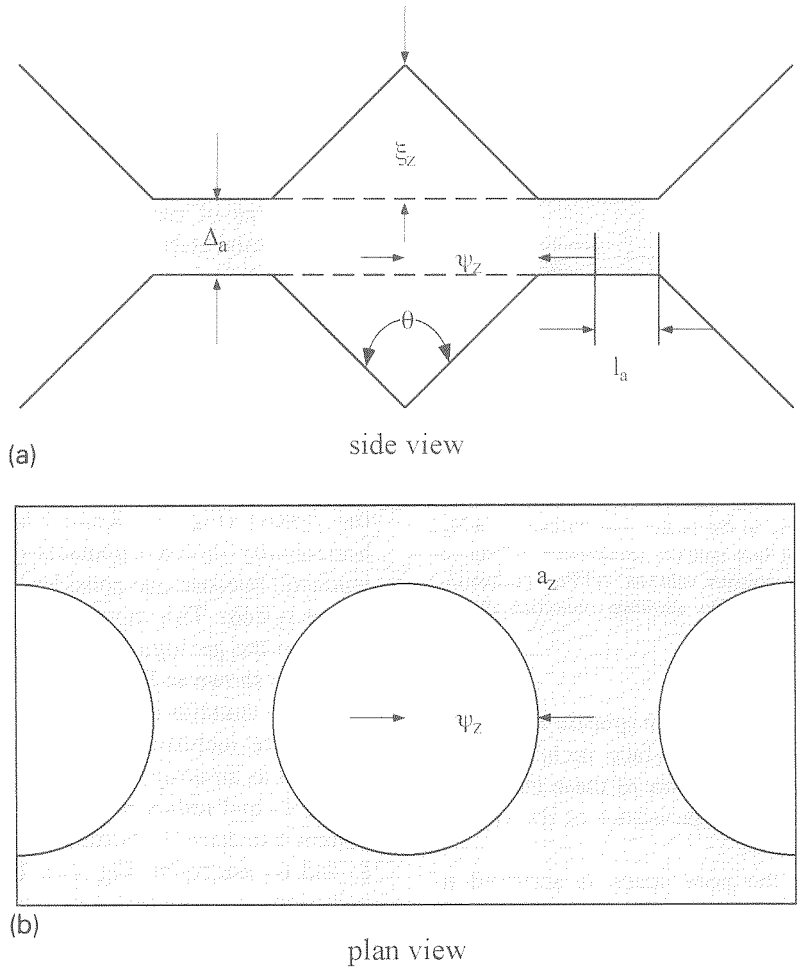

Fig. 4. (a) An expanded vertical cross-sectional view of a nominal contact containing actual true contacts and inclusions (free-face contacts). The contact area is filled by a water film of thickness Δ_a, and the inclusions are defined by conical shapes. (b) Horizontal view section of Fig. 4a passing through the center of the water film. The variables shown here are used in Eqs. 2A and 2B and following.

- $\underline{\underline{\sigma}}$ stress tensor at one point of the grain surface (bar).
- σ_z nominal stress normal to the nominal contact (bar).
- σ_a normal stress across an actual true contact (bar).
- σ_z^m macroscopic vertical stress (equivalent to a lithostatic stress) (bar).
- p_f fluid pressure within the free-face inclusion parts of the contact between the actual contacts (bar).
- Δ_a thickness of the water film in an actual contact (m).
- D_f effective diffusion coefficient for migration along the nominal z-contact ($m^2\ s^{-1}$).
- D_a diffusion coefficient for migration along an actual contact ($m^2\ s^{-1}$).
- D_p diffusion coefficient of water in the pore fluid ($m^2\ s^{-1}$).
- ξ_z height of a free-face inclusion contact (m), see Fig. 4.
- ψ_z radius of a free-face inclusion contact (m), see Fig. 4.
- l_a half of the distance between the free-face inclusion contacts (m).
- θ angle of aperture of the conic free-face inclusion contacts, $\theta = 2 \arctan(\xi_z/\psi_z)$

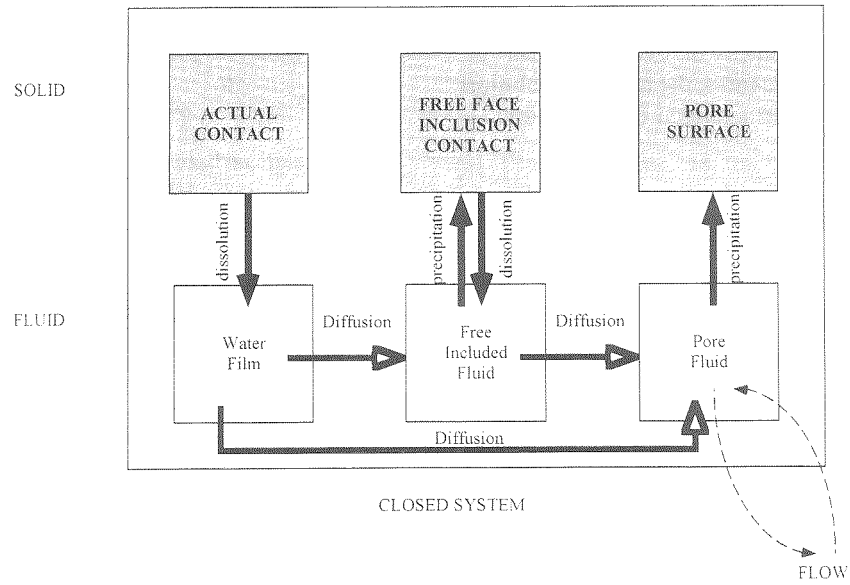

Fig. 5. Transitional pressure solution model. Dissolution occurs on the actual true contact sites. The solutes are then transported by diffusion along the water film to the free-face contacts and the pore space where they can precipitate. Simultaneously, matter can diffuse from the free-face contacts to the pore where it can precipitate. The system is closed at the grain scale. If there are exchanges inside the pore fluid with neighboring sediment through diffusion or advection, the closed system constraint is relaxed.

Three concentrations enter the model of contact dynamics:

c^p concentration of aqueous silica in the pore fluid (mole m^{-3}).
c^f concentration of aqueous silica in a free-face inclusion contact (mole m^{-3}).
c^a concentration of aqueous silica in the center of an actual contact (mole m^{-3}).

3.2. Geometrical evolution during deformation at a grain scale

The velocities G_a and G_f (m s^{-1}), defined in Figs. 2–4, describe the geometric evolution of the z-contact length variables. G_a, which is based on WFD, and G_f, which describes FFPS, are representative of the time evolution of the moving grain interface (Fig. 6). A third rate, G_p (m s^{-1}), takes

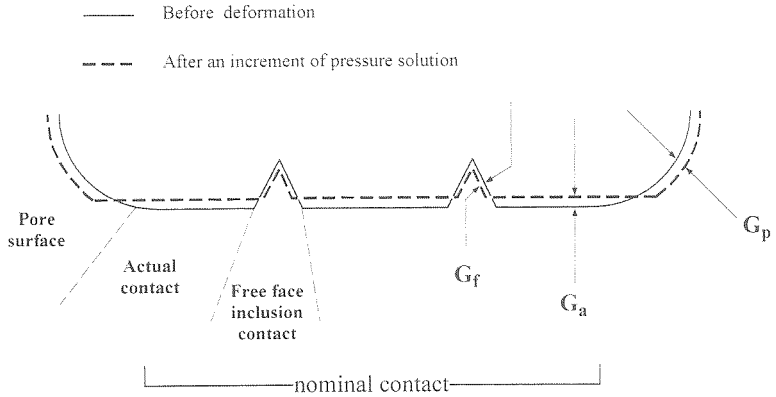

Fig. 6. View of the grain surface before and after an increment of pressure solution. The rates G_a, G_f, and G_p correspond to the velocity of the moving interface, see Eqs. 1, 2A, 2B and 3.

into account the evolution of the grain radius, L_f, and represents the thickness of overgrowth on the pore surface. Given these rates, the textural evolution of the grains can be characterized by the following assembly of equations:

$$\frac{dL_z}{dt} = G_a(c^a, \sigma_a, \sigma_z) \tag{1}$$

$$\frac{d\xi_z}{dt} = \begin{cases} \dfrac{G_a(c^a, \sigma_a, \sigma_z)}{\tan\left(\dfrac{\pi-\theta}{2}\right)} - \dfrac{G_f(c^f, p_p, \sigma_z)}{\sin\left(\dfrac{\pi-\theta}{2}\right)}, & \xi_z > 0 \\ 0, & \xi_z \le 0 \end{cases} \tag{2A}$$

$$\frac{d\psi_z}{dt} = \begin{cases} G_a(c^a, \sigma_a, \sigma_z) - \dfrac{G_f(c^f, p_p, \sigma_z)}{\sin\left(\dfrac{\theta}{2}\right)}, & \psi_z > 0 \\ 0, & \psi_z \le 0 \end{cases} \tag{2B}$$

$$\frac{dL_f}{dt} = G_p(c^p, p_p, \sigma_z) \tag{3}$$

where L_f is the grain radius, L_z is the length of the truncation of the spherical grain (Figs. 1 and 2), and ψ_z and ξ_z are respectively the radius and the height of the free-face inclusion contacts (Fig. 4). The variables G_a and G_f give the rate of change of the length variables characterizing the two sites inside a nominal contact. Rates are defined positive when dissolution occurs on the surface and negative for precipitation. Note that in Eqs. 2A and 2B the dynamics associated with the free-face inclusion contact sites, because of our geometrical model, depend on both WFD and FFPS rates.

In the model c^a is related to c^f by a steady state assumption (Dewers and Ortoleva, 1990). Letting l_a be the minimum distance between the network of holes (Fig. 4a), Fick's Law gives:

$$\frac{2\pi l_a \Delta_a D_a (c^a - c^f)}{l_a} = -\frac{a_z}{\overline{V}_s} G_a \tag{4}$$

$$\pi l_a^2 = a_z \tag{5}$$

where $\overline{V}_s$ is the molar volume of quartz (22.688×10^{-6} m^3 mole^{-1}). From Eq. 4:

$$c^a = c^f - \frac{a_z}{2\pi \Delta_a D_a \overline{V}_s} G_a \tag{6}$$

The relation between c^f and c^p is also obtained in the present model by a steady state assumption. However, the consideration is more complex because material can exchange not only with the pore fluid but also with the actual contacts (Fig. 5). Fick's Law gives:

$$\frac{2\pi l_z (\xi_z + \Delta_a/2) D_f (c^f - c^p)}{l_z} = -\frac{1}{\overline{V}_s}\left[n_z a_z G_a + (1 - n_z a_z) G_f\right] A_z \tag{7}$$

$$\pi l_z^2 = A_z \tag{8}$$

where $2(\xi_z + \Delta_a/2)$ is the thickness of the water layer in the free-face inclusion contact. We have used the fact that $n_z a_z$ is the fraction of the nominal contact area which is actual true contact (WFD) while $(1 - n_z a_z)$ is the free-face fraction area (FFPS). D_f is assumed to contain a tortuosity factor associated with the need to avoid the actual contacts while migrating to the pore. This tortuosity coefficient depends on the fraction between the actual contacts area and the nominal contact area with a power exponent (Turcotte, 1992). For continuity of the transition between pure WFD and FFPS dynamics one must have:

$$n_z a_z \to 1 \text{ and } a_z \to A_z \text{ as } \xi_z, \psi_z \to 0 \tag{9}$$

Thus the relationship between the actual fraction and the free-face fraction areas is:

$$n_z a_z = 1 - \pi n_z \psi_z^2 \tag{10}$$

Finally, we must take into account the conservation of volume in a closed system:

$$n_z a_z G_a + n_z \left(\pi \psi_z \sqrt{\psi_z^2 + \xi_z^2}\right) G_f + A_p G_p = 0 \tag{11}$$

In Eq. 11, the factor in front of G_f is the surface area of the conic inclusions constituting the free-face inclusion contacts. The rate G_p represents the precipitation on the pore surface (Fig. 6) which is equal to:

$$G_p = k_p \left(1 - \frac{c^p}{K_{eq}}\right) \tag{12}$$

where k_p is the rate of quartz precipitation and K_{eq} the equilibrium constant for quartz. The ratio in Eq. 12 represents the degree of saturation.

If the size of the inclusions becomes as small as the thickness of the water film, the above equations are no longer valid because the influence of G_f vanishes as the free-face inclusion contacts default to zero. In this case two processes continue to operate, one is the diffusion along the water film to the pore, the other is the conservation of aqueous silica. The whole dynamics is described by the following two equations:

$$\frac{2\pi l_z \Delta_a D_a (c^a - c^p)}{l_z} = -\frac{A_z}{V_s} G_a \tag{13}$$

$$A_z G_a + A_p G_p = 0 \tag{14}$$

4. Stresses at different sites

4.1. Normal stresses

For the monomineralic system modeled as a periodic array of truncated spheres, the following equation allows a feedback between pressure and rock texture. In Eq. 15 is described the relationship among the macroscopic vertical stress (equivalent to a lithostatic stress, for example the effect of overburden), σ_z^m, the normal stress on a nominal contact, σ_z, and the pore pressure, p_p (Dewers and Ortoleva, 1990, eq. 6):

$$-L_x L_y \sigma_z^m = A_z \sigma_z + \left(L_x L_y - A_z\right) p_p \tag{15}$$

Eq. 15 represents a force balance equation that couples rock texture and stress. As the grain contact surface area changes during deformation, the local stresses normal to the actual contact and normal to the free-face inclusion contacts are modified.

There is also a relationship between the effective microscopic normal stress on a nominal contact, σ_z, the normal stress on an actual true contact, σ_a, and the normal stress on a free-face inclusion contact, p_f (Fig. 3):

$$A_z \sigma_z = n_z a_z A_z \sigma_a + (1 - n_z a_z) A_z p_f \tag{16}$$

The normal pressure at the free-face inclusion contacts should range between p_p and σ_a. If the free-face inclusion contacts are directly connected and form channels, fluid pressure inside is the pore pressure. In contrast, when all the inclusions are closed, their internal pressure should increase and should reach a value close to the pressure on the actual true contacts. Two different relationships can be used to evaluate the fluid pressure inside the free-face inclusion contacts: (1) the normal stress is equal to the pore pressure; (2) the normal stress can vary between the pore pressure and the normal stress in the actual true contacts in a transitory way. Inclusions can be connected for a while, then they can seal themselves. Therefore, their internal pressure can vary during deformation. To model this process, we can use a geometrical interpolation such as when the free-face inclusion size decreases, p_f goes to σ_a; and when the inclusion size is increased, fluid inclusions are connected to the pore and p_f goes to p_p. This relationship, similar to a percolation law (Turcotte, 1992), gives another feedback between stress and geometry:

$$p_f = \sigma_a - (\sigma_a - p_p) \left(\frac{A_z - n_z a_z}{A_z}\right)^3 \tag{17}$$

When inclusions are connected, the geometry of the grain contact is assumed to be similar to an island-and-channel model (Spiers and Schutjens, 1990). The two values for the internal pressure (constant and transitory following Eq. 17) inside the inclusions will be compared in the numerical model (Fig. 9).

It remains to specify the variation of n_z (the number of free-face inclusion contacts per nominal contact). Here, it is assumed to be fixed by its original value at the moment of sedimentation although it might be argued that n_z should vary with ξ_z, Ψ_z (and other variables), and reaction progress. Typical values for n_z are comparable to dislocation densities on a mineral surface, ranging from 10^8 to 10^{12} per cm^2 in quartz, depending on the state of strain of the crystal (Wintsch and Dunning, 1985).

4.2. Stress tensors at the different sites

The stress tensor varies at the different sites over the grain surface: on the actual contact surface, on the free-face inclusion contact surface, and on the pore surface. In these sites, we have already defined the normal stress; it remains to specify the stresses in

Table 1
Stress tensor at the solid/liquid interface normal to z–axis; by definition compressive stresses are negative

Actual true contact	Free-face contact	Pore surface
$\begin{pmatrix} -\sigma_a & & \\ & -\sigma_a & \\ & & -\sigma_a \end{pmatrix}$	$\begin{pmatrix} -\sigma_a & & \\ & -\sigma_a & \\ & & -p_f \end{pmatrix}$	$\begin{pmatrix} -\sigma_z & & \\ & -\sigma_z & \\ & & -p_p \end{pmatrix}$

the two other directions to evaluate the stress tensors and the elastic contributions to the Helmholz free energy of the solid.

We assume the following stress tensors at the solid/liquid interface in the three sites (Table 1). In the actual contact the stresses in the three directions are equal to the actual stress σ_a . Inside the free-face inclusion contacts, the normal stress is defined in Eq. 17 and the stresses in the two other directions are as in the actual true contacts, i.e. σ_a. In the pore, the normal stress is the pore pressure, the two other stresses are equal to σ_z, the normal stress at a nominal z-contact.

5. Chemical potentials of quartz at different sites

The state of stress of a solid has a significant effect for its chemical potential. The effect is to increase the molar free energy of a stressed solid compared to that at zero-stress state (Sprunt and Nur, 1976; Heidug and Lehner, 1985). Though the Gibbs-type free energy cannot be defined for nonhydrostatically stressed solids (Shimizu, 1995, 1997), dissolution/precipitation of solids can be fully described by the surface chemical potential μ (Kamb, 1959; Gibbs, 1961; Paterson, 1973; Shimizu, 1995, 1997). If tangential stress on the grain surface is zero, the chemical potential can be written:

$$\mu = f + P_n \overline{V}_s \tag{18}$$

where μ is the chemical potential of the solute component, P_n is the normal pressure on the solid; it varies at the three sites of our model. f represents the molar Helmholz free energy. $\overline{V}_s$ is the molar volumes of the quartz under stress. Eq. 18 characterizes the chemical potential of quartz at each point on the surface of the solid and varies over the grain surface. The driving force for material transfer along a grain surface is the difference in chemical potential between two parts of the same crystal surface. If the compressibility of the solid is neglected, this difference can be written (Shimizu, 1995):

$$\Delta\mu = \Delta f + \overline{V}_s \Delta P_n \tag{19}$$

where Δ denotes a difference from a reference state and P_n is the normal stress on the solid. The term Δf contains contributions due to elastic energy, dislocation energy and surface energy. These different contributions are explained in the following.

5.1. Elastic energy

The elastic strain energy, U_e, depends on the stress tensor on the surface, $\underline{\underline{\sigma}}$ (given in Table 1), the molar volume of the solid, $\overline{V}_s$, the pore pressure, p_p, and the elastic compliance of the solid, $\underline{\underline{S}}$ (about 100 GPa for quartz) (Paterson, 1973; Reuschlé et al., 1988):

$$\Delta U_e \approx \frac{\left(\sigma^2 - p_p^2\right)\overline{V}_s}{2S} \tag{20}$$

The term σ in Eq. 20 is equal to $-\mathrm{tr}(\underline{\underline{\sigma}})/3$, where the stress tensors, $\underline{\underline{\sigma}}$, are defined at the different sites in Table 1. Among all the effects considered, the elastic contribution on the free energy is the smallest one (Table 2).

5.2. Effect of dislocation and plastic energy

Dislocations inside a crystal contribute to the definition of its internal energy. For high densities of dislocations (more than 10^{16} m^{-2}), the free energy of the solid can be increased significantly, which in turn increases the chemical potential of minerals and thus their solubility. If one assumes that the variation of the free energy of a crystal of quartz is only due to dislocation energy, U_d, one can calculate its contribution to the increase in silica chemical potential. For example, at 400°C and 3000 bar, the increase of quartz solubility is 1% if $\rho = 10^{14}$

Table 2
Effect of the different energies (J mole^{-1}) on the increase of the equilibrium constant of aqueous silica along the grain surface

Site	Normal stress effect (J mole^{-1})	ΔU_d (J mole^{-1})	ΔU_e (J mole^{-1})	ΔU_s (J mole^{-1})	Total effect on the increase of K_{eq}
Actual contact	+1658	+3	+2.5	0	+86%
Free-face contact	+283 to +1658	+170	+1.5	−4 to −40	+18 to +100%
Pore surface	+283	+3	+0.3	0	+11%

The equilibrium constant of reference is for an unstrained and unstressed quartz with a negligible surface energy. The plastic energy due to dislocations (U_d) is taken from Wintsch and Dunning (1985). The elastic energy, U_e, is calculated from Eq. 20. The surface energy, U_s, is calculated from Eq. 22. The stress was chosen to be a typical overburden value at 2 km depth, with lithostatic and hydrostatic gradients (the pore pressure equals 200 MPa); the temperature is 50°C and the grain size is 1.0 mm.

m^{-2} and 30% if $\rho = 10^{16}$ m^{-2}, where ρ is the dislocation density (Wintsch and Dunning, 1985). In clean moderately deformed quartz, ρ is not larger than 10^{13} m^{-2}, which is not sufficient to induce a significant chemical effect. On the contrary, in highly strained rocks, ρ can be increased by 2 or 3 orders of magnitude and the increase of U_d (which can reach 800 J/mole) can be sufficient to promote quartz dissolution.

At the microscopic scale of the grain surface, the free-face inclusion contacts should localize in the areas of higher dislocation density. We therefore assume that ρ is higher in the free-face inclusion contacts than in the actual contacts. In the simulations, we have chosen ρ to be 10^{15} m^{-2} in the free-face inclusion contacts and 10^{13} in the actual true contacts. These values correspond to dislocation energies of 170 kJ/mole and 3 kJ/mole, respectively (Wintsch and Dunning, 1985) (see Table 2).

5.3. Surface free energy

The surface free energy of a solid is the work needed to produce a unit of new surface by a reversible work yielding one equilibrium surface:

$$\gamma = \left(\frac{\partial G}{\partial A}\right)_{P,T} \tag{21}$$

The part of this energy in the total energy of the solid can be written as:

$$\Delta U_s = \frac{2\gamma \overline{V}_s}{r} \tag{22}$$

where r is the mean radius of curvature and $\overline{V}_s$ the molar volume of the solid.

The interfacial energy γ between quartz and liquid water is estimated to be $\gamma = 0.35$ J m^{-2} (Parks, 1984). This value is small so the surface energy effect is almost zero for particles bigger than about 0.5 μm. The surface energy creates a solubility variation which is controlled by the size of the particle. Hunter (1986, p. 268) gives the following relationship between γ and the activity:

$$\ln\left(\frac{a}{a_0}\right) = \frac{2\gamma \overline{V}_s}{rRT} \tag{23}$$

where a and a_0 are the activities of the solid with and without surface energy, γ is the surface energy, $\overline{V}_s$ is the molar volume of the solid, R the gas constant, T the temperature, and r the radius of the particle (if it is assumed that the two principal radii of curvature are equal).

In our model the fluid inclusions in the free-face inclusion contact area can reach sizes where a negative surface energy can become important. Eq. 23 permits to evaluate this decrease in activity of quartz, which is −5% for a 0.1 μm radius inclusion and −50% for 0.01 μm inclusions. Note that we neglect here the effects of pH and salinity on the surface energy although they can modify γ by a factor of 2 or 3 (Parks, 1984).

Hickman and Evans (1991) have reported experiments where deformation was measured at the contact between polished lenses of halite and/or quartz. They have observed no convergence when two lenses of halite were in contact but an increase of the surface area of contact between the lenses due to 'neck growth'. The driving force for this process of transport in the pore fluid is a gradient of surface curvature along the surface of the lens in contact

with the pore fluid (Hickman and Evans, 1991). This gradient induces a redistribution of material along the surface of the lenses. This mechanism will not be incorporated in our model of grain deformation because, on a long time scale, it cannot induce grain convergence and cannot modify a lot the porosity of a rock.

5.4. Total energy in the different sites and driving force for pressure solution

For the three sites used in this model the chemical potentials are different, thus the equilibrium constant of quartz, K_{eq}, varies, allowing for the chemical diffusive flux of mass from one site to another. From Eqs. 18–23, the chemical potential of quartz is:

$$\mu_{qz} = \mu_0 + \Delta P_n \overline{V}_s + \Delta U_e + \Delta U_d + \Delta U_s \qquad (24)$$

where μ_0 is the chemical potential for an unstrained crystal of quartz with negligible surface and strain energies under hydrostatic pressure P_n. In the model, the value of ΔP_n varies along the grain surface. It is $(\sigma_a - p_p)$ in the actual true contacts and $(p_f - p_p)$ in the free-face inclusion contacts.

By definition $\mu_{qz} = RT \ln(K_{eq})$, thus the equilibrium constant varies along the grain surface. At each site:

$$K_{eq} = K_0(T) \times \exp\left(\frac{\Delta P_n \overline{V}_s}{RT}\right) \times \exp\left(\frac{\Delta U_e}{RT}\right) \times \exp\left(\frac{\Delta U_d}{RT}\right) \times \exp\left(\frac{\Delta U_s}{RT}\right) \qquad (25)$$

where $K_0(T)$ is the equilibrium constant for an unstrained and unstressed solid whose value depends most only on temperature. In Table 2 the different energies have been categorized for their effects on the equilibrium constant.

Eq. 24 allows estimating the potential drop between the sites of dissolution and the sites of precipitation over the grain surface. The driving force for the multi-step pressure solution mechanism can be written in terms of a 'solubility difference' along the grain surface. If pressure solution is limited by the dissolution at the contact, the solubility difference acts as an undersaturation in the kinetics law of dissolution at grain contacts. If pressure solution is limited by diffusion along the actual contacts, the solubility difference gives a gradient of concentration between the grain contact and the pore (Fick's Law). And, if pressure solution is limited by precipitation in the pore, the solubility difference can be written as a supersaturation in the pore fluid (de Meer and Spiers, 1995).

6. Structure and properties of the adsorbed water film

6.1. Existence and thickness of a water film

Experimental evidences show that a water film can be trapped between minerals (Pashley and Kitchener, 1979; Pashley and Israelachvili, 1984; Horn et al., 1988, 1989). The thickness of this film has been measured or calculated for many minerals and varies from a few ångstroms to several nanometers (Peschel and Aldfinger, 1971; Heidug, 1995). Under most basin conditions its thickness decreases exponentially with stress until the lower limit of 0.5 nm is reached which represents the thickness of two layers of water molecules (Renard and Ortoleva, 1997).

The main physical origin of this physical dependency is electric surface charge, and the stability of the film is through an osmotic/Debye–Hückel model (Renard and Ortoleva, 1997). The stability of this fluid film can also be due to hydration forces (Heidug, 1995). In Fig. 7 the thickness of the water film is calculated as a function of the effective pressure, i.e., the amount by which the fluid pressure acting on the fluid–solid interface exceeds the hydrostatic pressure in the bulk fluid. The curves, for different surface charge on the mineral, indicate that the water film thickness is smaller between two grains of quartz than between two micas and depends therefore on the rock mineralogy.

6.2. Diffusion along the water film

The diffusion coefficient within the actual grain contact area is poorly determined. We believe it is not constant and should vary with the water film thickness Δ_a such that when Δ_a is thick enough the diffusion process should be that in free water. When the water film is only a few ångstroms thick, diffusion is expected to be like that in solid. This

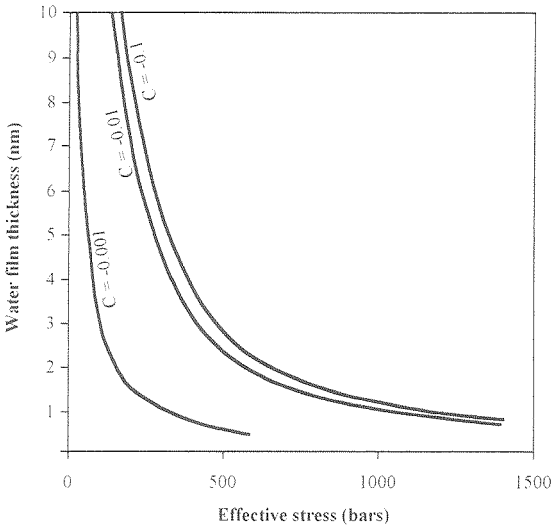

Fig. 7. Water film thickness between two grains as a function of effective stress and surface charge C (coulomb m^{-2}) of the mineral surface (Renard and Ortoleva, 1997). Typical value of the surface charges are -0.01 C m^{-2} for quartz and -0.1 C m^{-2} for mica. This difference allows the preservation of a bigger water film between two mica sheets than between two grains of quartz.

coefficient is important in our model because it controls the WFD rate compared to the FFPS one.

The diffusivity of a particle in a large volume of liquid is described by the Stokes–Einstein equation (Hunter, 1986):

$$D = \frac{kT}{6\pi\eta\delta} \tag{26}$$

where D is the diffusion coefficient ($m^2\ s^{-1}$), k the Boltzmann constant (1.38×10^{-23} m^3 Pa s^{-1}), δ the size of the particle, and η the viscosity of the liquid (Pa s). Horn et al. (1989) have measured the viscosity of a 2-nm water film trapped between silica sheets and found a value in the order of magnitude of 10^{-3} Pa s. Taking for δ the diameter of a molecule of hydrated silica to be 0.5 nm, the diffusion coefficient of silica inside a 2-nm water film at 25°C is therefore 3.5×10^{-10} $m^2\ s^{-1}$, within an order of magnitude less than diffusion in free water (Mullis, 1993).

Other authors have deduced the product coefficient of diffusion times water film thickness from pressure solution experiments and found results from 10^{-19} (Gratier and Guiguet, 1986; Spiers et al., 1990; Gratier, 1993) to 10^{-21} $m^3\ s^{-1}$ (Rutter, 1976). Their experiments are made at high effective stress, so the water film thickness should not exceed 0.5 nm, which corresponds to two layers of water molecules. Thus, assuming an activation energy of 15 kJ $mole^{-1}$, the diffusion coefficient of a water film of 0.5 nm thick can be estimated and found to range from 8×10^{-12} to 8×10^{-15} $m^2\ s^{-1}$ at 25°C, which is in good agreement with values reported by Nakashima (1995). Despite the wide range of these values, they are several orders of magnitude higher than that for diffusion in solids (Freer, 1981).

A small value of the coefficient of diffusion is necessary to maintain the stability of the free-face inclusions and allows the FFPS mechanism to operate. The coefficient of diffusion along the water film D_a is chosen to be such that it decreases with Δ_a to take into account the former observations. When the water film is thick enough ($\Delta_a > 5$ nm) the diffusion is that in free water, i.e. the coefficient of diffusion is equal to 2×10^{-9} $m^2\ s^{-1}$ at 25°C (Applin, 1987); and when the water film thickness falls to 0.5 nm, the coefficient decreases to 10^{-14} $m^2\ s^{-1}$ at 25°C (Nakashima, 1995). We have calibrated the coefficient of diffusion such as it takes into account these observations and found:

$$D_a = D_{a.min} + \left(D_p - D_{a.min}\right) \times \frac{1}{1 + \exp\left(-\dfrac{\Delta_a - 25 \times 10^{-10}}{2.5 \times 10^{-10}}\right)} \tag{27}$$

where $D_{a.min}$ equals 10^{-14} $m^2\ s^{-1}$ at 25°C. With Eq. 27), the coefficient of diffusion takes into account the high diffusivity in free water (Applin, 1987), the medium diffusivity in a 2-nm-thick water film (Horn et al., 1989) and the low diffusivity in a 0.5-nm film (Rutter, 1976; Gratier and Guiguet, 1986). All of these coefficients of diffusion are assumed to have an activation energy of 15 kJ $mole^{-1}$.

The effective diffusion coefficient between the free-face inclusion contact and the pore, D_f, must be addressed for two effects. First, diffusion is more difficult than in free water because of the obstructions imposed by the actual true contacts. Second, diffusion is easier than along the water film because the free-face inclusion contacts are wider and can be connected to form small channels where diffusion is promoted. Here we assume that the variable that

controls diffusion is the ratio between the free-face surface area and the nominal surface area through:

$$D_f = D_a + (D_p - D_a)\left(\frac{(1 - n_z a_z)A_z}{A_z}\right)^{\alpha} \quad (28)$$

A typical choice for α is 3, based on percolation modeling (Turcotte, 1992).

7. Model testing and calibration

7.1. Solubility of quartz

In the model, the chemical reaction of dissolution or precipitation of quartz is taken to be:

$$SiO_{2(s)} + 2H_2O \Leftrightarrow H_4SiO_{4(aq)}$$

The equilibrium constant K_{eq} for this reaction is:

$$K_{eq} = \frac{a_{H_4SiO_4}}{a_{SiO_2} a_{H_2O}} \quad (29)$$

where all the a's are the activity of the species in solution.

At equilibrium, if we take the reference states of solid quartz and water to be pure states under stress states considered, the activities of quartz and water are equal to 1. The equilibrium constant is related to silica solubility $c_{H_4SiO_4}$ through:

$$K_{eq} = \gamma_{H_4SiO_4} c_{H_4SiO_4} \quad (30)$$

where $\gamma_{H_4SiO_4}$ is the activity coefficient, assumed to be equal to 1 in a dilute pressure free state. K_{eq} under stress is related to the equilibrium constant K_0 in stress-free state by:

$$K_{eq} = K_0 \exp\left(\frac{\mu_{qz} - \mu_0}{RT}\right) \quad (31)$$

Using these relation and Eq. 25, one can estimate the solubility in the different sites. In Eq. 25, $K_0(T)$ is almost only dependent on temperature (Rimstidt and Barnes, 1980; Rimstidt, 1997). It is the equilibrium constant for a stress-, dislocation-, elastic- and surface energy-'free' state. We choose its value to be as follows (Rimstidt and Barnes, 1980):

$$\log(K_0) = 1.881 - 0.002028 \times T - \frac{1560}{T} \quad (32)$$

7.2. Kinetics of dissolution/precipitation

The rate constant for dissolution/precipitation increases with temperature and varies with pH and ionic concentrations (Dove, 1994). Some authors have evaluated the kinetics of quartz dissolution through laboratory measurements (Rimstidt and Barnes, 1980; Brady and Walther, 1990; Dove, 1994) and found rates faster than in geological conditions (Oelkers et al., 1996). Walderhaug (1994) has estimated precipitation rates in sandstones in the Norwegian shelf from fluid inclusion microthermometry and he has found a value much lower. Because of the large uncertainty about the kinetics of quartz dissolution/precipitation, we have chosen to calibrate our model with kinetics which are able to take into account geological observations of porosity–depth curves in sandstones (Ramm, 1992). We have tried several models and the values of the kinetics constant which best fit the geological data are those of Brady and Walther (1990) which give intermediate values for quartz kinetics of dissolution and precipitation.

7.3. Initial geometry of the grains and contacts

A range of grain sizes was investigated. For example, in North Sea sandstones, the typical grain size is between 0.1 and 1 mm. The initial size of the free-face inclusions inside the nominal contact is set to be equal to 1 μm. This value is chosen to represent the initial roughness of the contact surface; it is a typical size of a fluid inclusion. The constant angle of the conic inclusions is chosen to be 90°, so $\xi_z = \psi_z$. The number of inclusions is fixed such that in a nominal contact, 50% of the surface area is actual true contact and initially deforms with WFD, whereas 50% of the surface area contain fluid inclusions and deform with a FFPS mechanism (Fig. 8c). During deformation, this ratio evolves.

Sedimentology presents an initial wide range of inclusion sizes inside the contact before deformation. Initial inclusions that do not contain dislocations have a smaller free energy than those located near dislocations. The former ones are consumed faster, whilst those with dislocations survive. Thus there exist preferred sites for inclusions within the contacts.

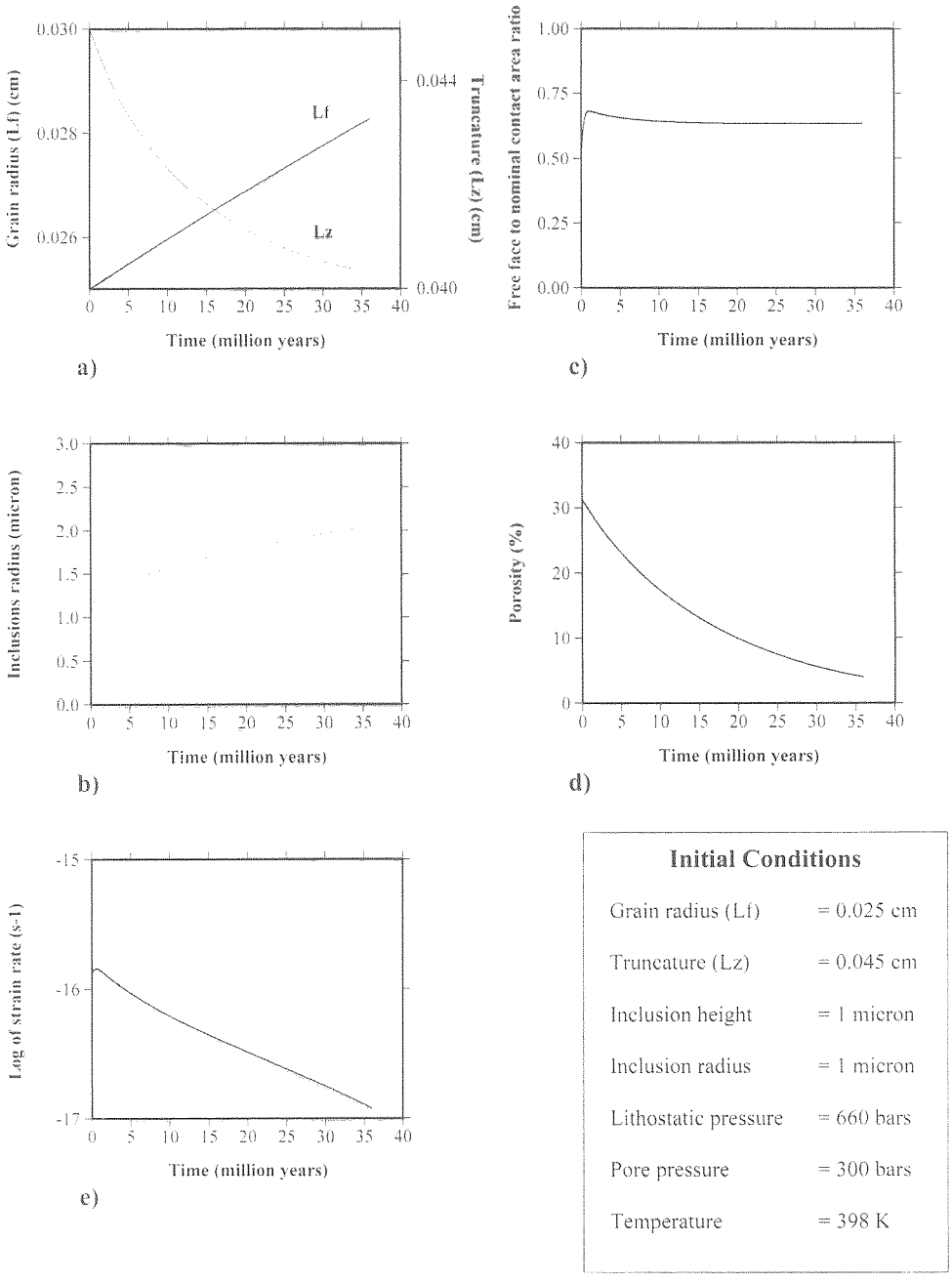

Fig. 8. Sandstone compaction by a pressure solution model. Constant temperature, pore pressure and lithostatic pressure were used for this simulation. One can observe the variations of the length variables (see Figs. 1 and 2 for their definitions): L_f (the grain radius) increases (Fig. 8a) while grain indentation implies the decrease of L_z (Fig. 8a). The overall grain volume is conserved. The free-face contact radius ξ_z increases during compaction (Fig. 8b). The ratio between the free-face contacts and the nominal contact areas evolves up to an equilibrium value equal to 65% in this simulation (Fig. 8c). During compaction, porosity decreases from 31% to 4% in 36 million years (Fig. 8d), and the vertical strain rate exponentially decreases (Fig. 8e) because of an increase of the surface area of the nominal contacts. Physical conditions are chosen to be similar to that of a sediment held at 2 km depth.

8. Results and discussion

8.1. Grain deformation and stability of the free-face inclusions

During chemical compaction, dissolution occurs inside the contact and matter precipitates on the pore surface, hence L_f (measuring the thickness of overgrowth on the pore surface) increases (Fig. 8a). In our model, it is assumed that chemical compaction is isotropic, so grain truncation lengths L_x, L_y, and L_z all decrease with deformation (Fig. 8a). The model is closed at the grain scale with respect to solid mass, thus the grain volume does not change with time. The grain evolves as a truncated sphere with decreasing pore surface area and increasing nominal contact area (Fig. 1). Simultaneously, porosity decreases (Fig. 8d).

The size of the free-face inclusions varies during deformation (Fig. 8b). They can increase because their internal fluid pressure is higher than the pore pressure and because they have some free energy stored in dislocations. They can decrease in size too with deformation, depending on the physical conditions.

The ratio between the free-face inclusions surface area and the nominal contact surface area (Fig. 8c) evolves in the same way as the inclusion size. This ratio is fixed initially at 50% and increases rapidly up to 70% in an early stage of deformation, then decreases slightly to the equilibrium value of 65% for the case of Fig. 8c.

The macroscopic vertical strain rate ε_v, defined as the rate at which the grains are shortening ($2G_a/L_z$) decreases during deformation (Fig. 8e) because the surface area of the nominal contacts increases, and thereby the local stress on the nominal contacts decreases. This fact is crucial because it shows that, as grain geometry evolves and if the rock stays in the same physical and chemical conditions, the strain rate does not stay constant. The total deformation observed on a sample of this rock is not produced at the same local strain rate. This fact has already been observed in experiments on pressure solution (Dewers and Hajash, 1995).

An important point for this rate of deformation is that it is slower than estimated by Shimizu (1995) by two orders of magnitude. This difference arises from the choice to use kinetics constants for quartz precipitation that fit geological data (Walderhaug, 1994), whereas rates measured in laboratory indicate faster kinetics (Dove, 1994).

8.2. Fluid pressure inside the fluid inclusions

Depending on the relationship chosen to estimate the fluid pressure inside the free-face inclusion contacts, the rate for porosity variation is not the same. If the pressure inside the fluid inclusions is equal to the pore fluid, i.e. if all the fluid inclusions are connected to the pore, the driving force for pressure solution in the free-face inclusion contacts is smaller than in the actual contacts. Therefore fluid inclusions tend to vanish because the rate of WFD on the actual true contacts is higher than the rate of FFPS in the inclusions. On the contrary, if the pressure inside the fluid inclusions is transitory, see Eq. 17, the fluid inclusions stay open and, as the mean distance for aqueous silica diffusion inside the nominal contact is small, the rate of deformation by pressure solution is accelerated (Fig. 9). In Figs. 8, 10 and 11, the transi-

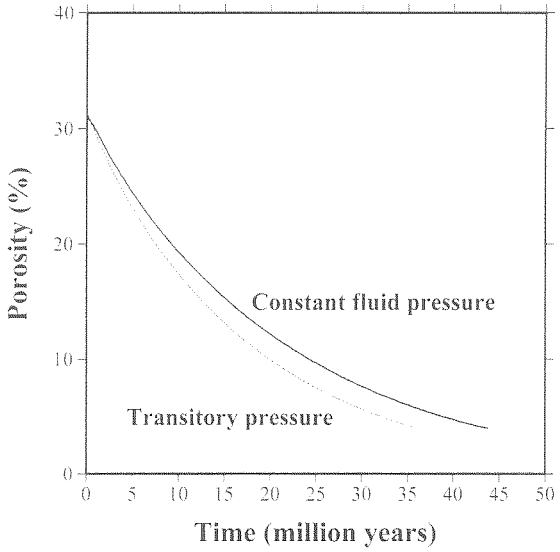

Fig. 9. Effect of the fluid pressure inside the free-face contacts. If the fluid pressure inside the free-face contacts is equal to the pore pressure (i.e. if all the fluid inclusions are connected to the pore) the rate of porosity decrease is smaller than in the case where the fluid pressure can vary in a transitory way (Eq. 17).

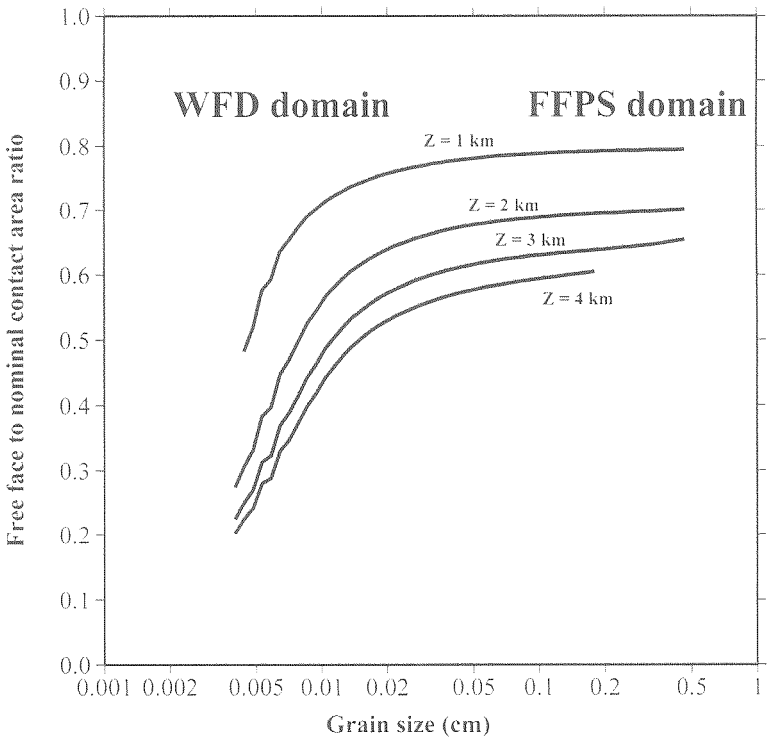

Fig. 10. Ratio between the free-face inclusion contact area and the nominal contact area as a function of grain size, for different depths. Each point on the curves corresponds to a simulation similar to that in Fig. 8, but for different grain size and depths. The initial porosity is chosen to be 31% and the steady state ratio is evaluated at the end of deformation when the porosity has reached 4% (as in Fig. 8c at 36 million years). For fine-grained sandstones, the ratio is negligible. It increases rapidly for grain size larger than 0.02 cm. This figure shows the shift between WFD and FFPS domains due to the decrease of diffusion rate with increased grain size. The different curves correspond to different depths, assuming lithostatic and hydrostatic pressure gradients, and a temperature gradient of 40°C km^{-1}.

tory pressure inside the fluid inclusions is chosen to obey Eq. 17.

8.3. The shifting between the WFD and FFPS fields

Simulations, similar to that in Fig. 8, have been performed for different grain sizes and physical conditions. When the porosity of the rock has reached 4%, the equilibrium value of the free-face ratio (Fig. 8c) is reported as a function of grain size and depth. For grain sizes smaller than 0.02 mm, the free-face ratio is small (Fig. 10). This ratio increases with grain size. Below the limit grain size, diffusion from the actual true contacts to the free-face inclusions is fast because of a short path length for diffusion. In this case the fluid in free-face inclusions reaches saturation, so the inclusions are not stabilized and vanish. As grain size gets bigger, the actual true contacts do also and diffusion inside the water film becomes less efficient, furthermore σ_a diminishes to σ_z (Eq. 17), decreasing the driving force for WFD, then the inclusion size increases and FFPS becomes dominant. The physical conditions are also important: free-face inclusions are less stable at greater depth because the stress on the actual true contacts is large and WFD is more efficient.

Simulations such as those in Fig. 10 suggest the existence of two distinct fields of deformation. For small grain size, the mechanism of deformation is only WFD (diffusion-limited), whereas for bigger grain size both FFPS (reaction-controlled) and WFD operate, the transition being at a grain size between 0.01 and 0.03 cm for quartz, depending on depth. Note that our model integrates these two regimes in a coupled way. As already pointed out by Shimizu (1995), conditions in the upper crust are such that the

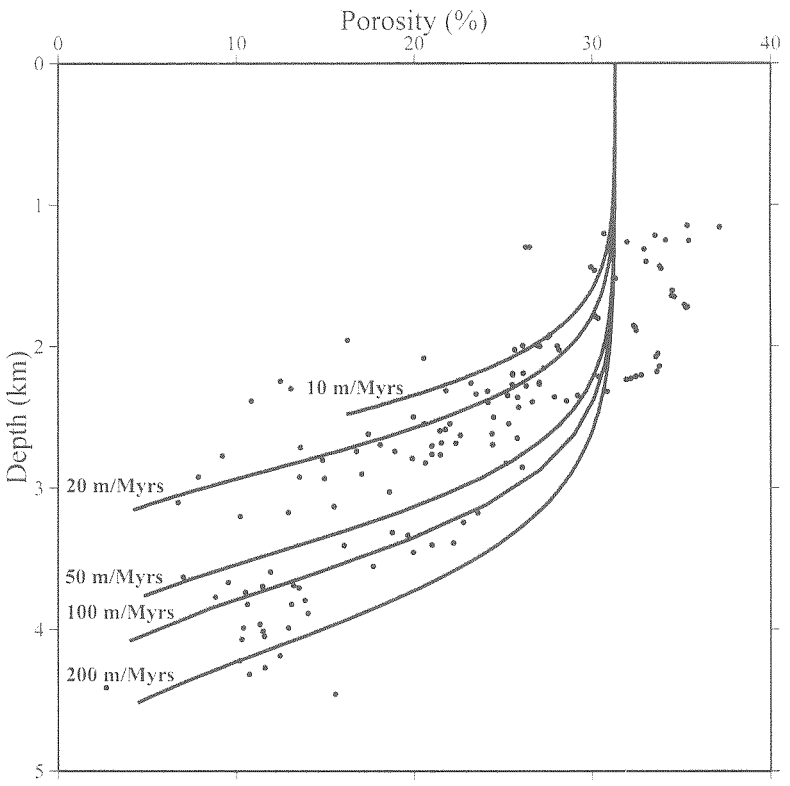

Fig. 11. Porosity–depth relationships in a sandstone. Dots represent data in sandstones from the Norwegian shelf (Ramm, 1992). The curves are porosity–depth relationships calculated with our model of pressure solution for different sedimentation rates. In the numerical model, a constant rate of sedimentation is assumed. Grain size, fluid pressure, and temperature gradient (35°C/km) are similar to that in the Norwegian shelf. Between 0 and 2 km, pressure solution is inefficient and its efficiency increases rapidly at around 3 km.

two regimes (reaction-limited and diffusion-limited) can coexist for quartz-rich sediments.

8.4. Effect of grain coating in pore space

Clay coatings can retard pressure solution (Tada et al., 1987; Ramm, 1992). In this case, quartz precipitation on the pore surface is hindered because of the loss of pore surface area in Eqs. 11 and 14. The pore fluid becomes supersaturated with silica so that the gradient of concentration between the nominal contact and the pore can disappear in Eqs. 7 and 13 and therefore the driving force for contact dissolution and diffusion is diminished. As a consequence, the rate of pressure solution by the mechanism 'water film diffusion' is diminished.

8.5. Interaction between pressure solution and the other mechanisms of deformation

In this study only the mechanism of pressure solution is considered as a process of compaction. It is well known that other mechanisms of deformation are also efficient and can interact with pressure solution: brittle deformation such as grain crushing or stress-corrosion cracking (Onasch and Dune, 1993) and plastic deformation (Pharr and Ashby, 1983; Tada et al., 1987). These mechanisms are efficient at higher strain rates than pressure solution.

After an episode of brittle deformation, the mean grain size of a rock is decreased. Therefore, distance for diffusion inside the grain contacts is lowered and pressure solution becomes more efficient. Interactions between pressure solution and grain crushing could explain fast rates of deformation as observed

for instance in indented pebbles (Mac Ewen, 1978; Gratier et al., 1999).

8.6. Case of an open system

In the calculations presented here, we are assuming that matter that goes outside the nominal contact precipitates on the pore surface, the system being closed with respect to solid mass at a grain scale. If the system is considered to be closed at a decimeter to meter scale, larger diffusive and advective transport phenomena should not be neglected (Lehner, 1995). Matter can diffuse from a region where pressure solution is inhibited due to coating effects to a region where grains are cleaner and overgrowths can form. Such a process can operate in sandstones where beds with abundant precipitated silica alternate with stylolite-rich regions where quartz dissolves (Oelkers et al., 1996). In these systems, the driving force for pressure solution is the same in the clean layers and in the stylolites while, in the latter, precipitation is slower due to clay coating. Furthermore, we believe that free-face inclusions should be more likely to be present in the clay-free zones than in the stylolitized ones because, in the latter, the presence of clays inside the contact between the grains is assumed to promote the WFD mechanism (Carrio-Schaffhauser et al., 1990; Bjørkum, 1996).

8.7. Application to sandstone compaction

Up to now, the pressure solution model we have described considers compaction for a rock at constant depth. Now we apply this model in sedimentary basin conditions, with a constant burial rate. The resulting 1D model allows to estimate porosity diminution with depth and time, at a constant sedimentation rate. This compaction model is applied for very simple conditions: constant rate of sedimentation (20 to 100 m per million years), hydrostatic and lithostatic pressure gradients, constant temperature gradient (35°C/km), and constant grain size sediment deposition (0.5 mm). We make the assumptions that there is no overpressured compartment in the basin, even if the hypothesis is far from reality (Ortoleva, 1994), and that porosity variation occurs only by pressure solution at a grain scale.

The numerical model allows calculating porosity–depth curves for different rates of sedimentation (Fig. 11). These curves represent the amount of compaction induced by pressure solution. Between 0 and 2 km, pressure solution compaction is very slow because temperature is low and quartz kinetics are very slow. In contrast, pressure solution becomes efficient below 2 to 3 km and porosity continually decreases with depth.

The curves are compared with data from the Norwegian margin (Ramm, 1992), where grain size, burial rates, and temperature gradient are similar to the simulated curves. The pressure solution curves do not represent porosity variations above 2 km because only mechanical compaction occurs at this depth (grain sliding, fracturation of low-resistance grains). Below 2 km, the numerical curves seem to fit the porosity–depth data trend.

9. Conclusion

This study shows that the different models of pressure solution that are described in the literature can be integrated into a unified model that incorporates three distinct processes: stress enhanced dissolution, transport by diffusion (in one or two steps), and precipitation.

The complex non-linear dynamics of pressure solution arises because of two main factors:

(1) Both grain geometry and rock texture evolve with time and interact with local stress over the grain surface.

(2) The mechanism of pressure solution can be divided in different successive steps, the slowest of which controlling the overall rate of deformation. During deformation and with grain geometry variations, this slowest step can vary in a transitory way. For example, compaction can be limited by reaction kinetics at one time and by diffusion along the interface at another. The transition appears with time because the rock texture changes with deformation and because the physical and chemical parameters vary during burial.

A transition between the two mechanisms of pressure solution (WFD and FFPS) occurs because of two factors. First the solute mobility inside the trapped water film between the grains decrease with increasing stress. Secondly inclusions inside the con-

tact between the grains should be localized in the areas of original high dislocation density.

The transitional pressure solution model is a combination of these effects and shows that 'water film diffusion', 'free-face pressure solution', and the model of islands and channels are natural consequences of both kinetic and free energy aspects of pressure solution.

Acknowledgements

This study was supported by the Institut Français du Pétrole, the CNRS (GdR Géomécanique des Roches Profondes), the Basic Energy Sciences program of the US Department of Energy (grant No. DE-FG02-91ER14175) and the Gas Research Institute (grant No. 5097-260-3779). We would like to thank Anne-Marie Boullier for helpful discussions. I. Shimizu and two anonymous reviewers as well as T. Engelder are thanked for their constructive comments.

References

Applin, K.R., 1987. The diffusion of dissolved silica in dilute aqueous solution. Geochim. Cosmochim. Acta 5, 2147–2151.

Bathurst, R.G.C., 1958. Diagenetic fabrics in some British Dinantian limestones. Liverpool Manchester Geol. 2, 11–36.

Bjørkum, P.A., 1996. How important is pressure in causing dissolution of quartz in sandstones? J. Sediment. Res. 66, 147–154.

Brady, P.V., Walther, J.V., 1990. Kinetics of quartz dissolution at low temperatures. Chem. Geol. 82, 253–264.

Carrio-Schaffhauser, E., Raynaud, S., Latiere, H.J., Mazerolle, F., 1990. Propagation and localization of stylolites in limestones. In: Knipe, R.J., Rutter, E.H. (Eds.), Deformation Mechanisms: Rheology and Tectonics. Geol. Soc. London, pp. 193–199.

de Meer, S., Spiers, C.J., 1995. Creep of wet gypsum aggregates under hydrostatic loading conditions. Tectonophysics 245, 171–183.

Dewers, T., Hajash, A., 1995. Rate-laws for water-assisted compaction and stressed-induced water–rock interaction in sandstones. J. Geophys. Res. 100, 13093–13112.

Dewers, T., Ortoleva, P., 1990. A coupled reaction–transport mechanical model for intergranular pressure solution stylolites, and differential compaction and cementation in clean sandstones. Geochim. Cosmochim. Acta 54, 1609–1625.

Dove, P.M., 1994. The dissolution kinetics of quartz in sodium chloride solutions at 25° to 300°C. Am. J. Sci. 294, 665–712.

Engelder, T., 1982. A natural example of the simultaneous operation of free-face dissolution and pressure solution. Geochim. Cosmochim. Acta 46, 69–74.

Freer, R., 1981. Diffusion in silicate minerals and glasses: a data digest and guide to the literature. Contrib. Mineral. Petrol. 76, 440–454.

Gibbs, J.W., 1961. The collected works of J. Willard Gibbs. Vol. 1. Thermodynamics. Yale University Press.

Gratier, J.P., 1993. Experimental pressure solution of halite by an indenter technique. Geophys. Res. Lett. 20, 1647–1650.

Gratier, J.P., Guiguet, R., 1986. Experimental pressure solution–deposition on quartz grains: the crucial effect of the nature of the fluid. J. Struct. Geol. 8, 845–856.

Gratier, J.P., Renard, F., Labaume, P., 1999. How pressure solution creep and fracturing process interact in the upper crust to make it behave as both brittle and viscous. J. Struct. Geol. (in press).

Gratz, A.J., 1991. Solution-transfer compaction in quartzites: progress towards a rate law. Geology 19, 901–904.

Gratz, A.J., Bird, P., 1993a. Quartz dissolution: negative crystal experiments and rate law. Geochim. Cosmochim. Acta 57, 965–976.

Gratz, A.J., Bird, P., 1993b. Quartz dissolution: theory of rough and smooth surfaces. Geochim. Cosmochim. Acta 57, 977–989.

Heald, M.T., 1955. Stylolites in sandstones. J. Geol. 63, 101–114.

Heidug, W.K., 1995. Intergranular solid–fluid phase transformations under stress: the effect of surface forces. J. Geophys. Res. 100, 5931–5940.

Heidug, W., Lehner, F.K., 1985. Thermodynamics of coherent phase transformations in nonhydrostatically stressed. PAGEOPH 123, 91–98.

Hickman, S.H., Evans, B., 1991. Experimental pressure solution in halite: the effect of grain/interface boundary structure. J. Geol. Soc. London 148, 549–560.

Horn, R.G., Clarke, D.R., Clarkson, M.T., 1988. Direct measurements of surface forces between sapphire crystals in aqueous solutions. J. Mat. Res. 3, 413–416.

Horn, R.G., Smith, D.T., Haller, W., 1989. Surface forces and viscosity of water measured between silica sheets. Chem. Phys. Lett. 162, 404–408.

Hunter, R.J., 1986. Foundations of Colloid Science. Oxford Science Publications, Oxford.

Kamb, W.B., 1959. Theory of preferred crystal orientations developed by crystallization under stress. J. Geol. 67, 153–170.

Lehner, F.K., 1995. A model for intergranular pressure solution in open systems. Tectonophysics 245, 153–170.

Mac Ewen, T.J., 1978. Diffusional mass processes in pitted pebble conglomerates. Contrib. Mineral. Petrol. 67, 405–415.

Mullis, A.M., 1993. Determination of the rate-limiting mechanism for quartz pressure dissolution. Geochim. Cosmochim. Acta 57, 1499–1503.

Nakashima, S., 1995. Diffusivity of ions in pore water as a quantitative basis for rock deformation rate estimates. Tectonophysics 245, 185–203.

Oelkers, E.H., Bjørkum, P.A., Murphy, W.M., 1996. A petrographic and computational investigation of quartz cementation

and porosity reduction in North Sea sandstones. Am. J. Sci. 296, 420–452.
Onasch, C.M., Dune, W.M., 1993. Variations in quartz arenite deformation mechanisms between sequence and duplexes. J. Struct. Geol. 15, 465–475.
Ortoleva, P.J., 1994. Geochemical Self-Organization. Oxford University Press, New York.
Parks, G.A., 1984. Surface and interfacial free energies of quartz. J. Geophys. Res. 89, 3997–4008.
Pashley, R.M., Israelachvili, J.N., 1984. Molecular layering of water in thin films between mica surfaces and its relation to hydration forces. J. Colloid Interface Sci. 101, 510–522.
Pashley, R.M., Kitchener, J.A., 1979. Surface forces in adsorbed multilayers of water on quartz. J. Colloid Interface Sci. 71, 491–500.
Paterson, M.S., 1973. Nonhydrostatic thermodynamics and its geologic applications. Rev Geophys. Space Phys. 11, 355–389.
Peschel, G., Aldfinger, K.H., 1971. Thermodynamic investigations of thin liquid layers between solid surfaces. Z. Naturforsch. 26, 707–715.
Pharr, G.M., Ashby, M.F., 1983. On creep enhanced by a liquid phase. Acta Metall. 31, 129–138.
Raj, R., Chyung, C.K., 1981. Solution-precipitation creep in glass ceramics. Acta Metall. 29, 159–166.
Ramm, M., 1992. Porosity–depth trends in reservoir sandstones: theoretical models related to Jurassic sandstones offshore Norway. Mar. Pet. Geol. 9, 553–567.
Renard, F., Ortoleva, P., 1997. Water film at grain–grain contacts: Debye–Huckel, osmotic model of stress, salinity, and mineralogy dependence. Geochim. Cosmochim. Acta 61, 1963–1970.
Renard, F., Ortoleva, P., Gratier, J.P., 1997. Pressure solution in sandstones: influence of clays and dependence on temperature and stress. Tectonophysics 280, 257–266.
Reuschlé, T., Trotignon, L., Gueguen, Y., 1988. Pore shape evolution by solution transfer: thermodynamics and mechanics. Geophys. J. 95, 535–547.
Rimstidt, J.D., 1997. Quartz solubility at low temperatures. Geochim. Cosmochim. Acta 61, 2553–2558.
Rimstidt, J.D., Barnes, H.L., 1980. The kinetics of silica–water reactions. Geochim. Cosmochim. Acta 44, 1683–1699.
Rutter, E.H., 1976. The kinetics of rock deformation by pressure solution. Philos. Trans. R. Soc. London 283, 203–219.
Schutjens, P.M.T., 1991. Experimental compaction of quartz sand at low effective stress. J. Geol. Soc. London 148, 527–539.
Shimizu, I., 1995. Kinetics of pressure solution creep in quartz: theoretical considerations. Tectonophysics 245, 121–134.
Shimizu, I., 1997. The nonequilibrium thermodynamics of intracrystalline diffusion under nonhydrostatic stress. Philos. Mag. A 75, 1221–1235.
Spiers, C.J., Schutjens, P.M.T.M., 1990. Densification of crystalline aggregates by fluid phase diffusion creep. In: Barber, D.J., Meredith, P.G. (Eds.), Deformation Mechanisms in Minerals, Ceramics and Rocks. Unwin Hyman, London, pp. 334–353.
Spiers, C.J., Schutjens, P.M.T.M., Brzesowsky, R.H., Peach, C.J., Liezenberg, J.L., Zwart, H.J., 1990. Experimental determination of constitutive parameters governing creep of rocksalt by pressure solution. In: Knipe, R.J., Rutter, E.H. (Eds.), Deformation Mechanisms, Rheology and Tectonics. Geol. Soc. Spec. Publ. 54, 215–227.
Sprunt, E.S., Nur, A., 1976. Reduction of porosity by pressure solution: experimental verification. Geology 4, 463–466.
Tada, R., Maliva, R., Siever, R., 1987. A new mechanism of pressure solution in porous quartzose sandstone. Geochim. Cosmochim. Acta 51, 2295–2301.
Turcotte, D.L., 1992. Fractals and Chaos in Geology and Geophysics. Cambridge University Press, Cambridge.
Urai, J., Spiers, C.J., Zwart, H.J., Lister, G.S., 1986. Weakening of rock salt by water during long-term creep. Nature 324, 554–557.
Wakai, F., 1994. Step model of solution-precipitation creep. Acta Metall. Mater. 42, 1163–1172.
Walderhaug, O., 1994. Precipitation rates for quartz cement in sandstones determined by fluid-inclusion microthermometry and temperature-history modeling. J. Sediment. Res. 64, 324–333.
Weyl, P.K., 1959. Pressure solution and the force of crystallization — a phenomenological theory. J. Geophys. Res. 69, 2001–2025.
Wintsch, R.P., Dunning, J., 1985. The effect of dislocation density on the aqueous solubility of quartz and some geologic implications: a theoretical approach. J. Geophys. Res. 90, 3649–3657.